

Time-resolved Spectroscopy of the M15 X-ray Binary AC211/X2127+119

M. A. P. Torres¹, P. J. Callanan¹, M. R. Garcia²

¹*Physics Department, University College, Cork, Ireland*

²*Harvard-Smithsonian Center for Astrophysics, 60 Garden St, Cambridge, MA 02138*

2 November 2018

ABSTRACT

We present time-resolved spectroscopy acquired during two epochs (spaced apart by ~ 15 days) of the eclipsing Low Mass X-ray Binary AC211/X2127+119 in the globular cluster M15. The spectra show variations in the HeII $\lambda 4686$ emission line not only modulated on the orbital period, but also on time-scales of a few days. During the first epoch of observation, the emission line shows a strong S-wave superimposed on the average double-peaked profile. The line exhibits no evidence of rotational disturbance at the orbital phases when the eclipse is observed in the optical continuum. During the second epoch, no double-peak or S-wave component is present. The HeI absorption lines detected by other authors are not present in our spectra. A Doppler image of the HeII $\lambda 4686$ for the first epoch supports the presence of the accretion disc. No hotspot is detected, although enhanced emission at $V_X = 30 \text{ km s}^{-1}$, $V_Y = 160 \text{ km s}^{-1}$ is observed. We discuss the implications of this emission in the context of an X-ray heated donor star, in which case a high mass ratio and neutron star primary are implied. Finally, we speculate on the possibility of a misaligned secondary star in AC211.

Key words: accretion, accretion discs – binaries: close – X-rays: binaries – stars: individual: AC211, X2127+119

1 INTRODUCTION

Low Mass X-ray Binaries (LMXBs) are systems which harbour an accretion disc through which mass from a low mass secondary ($M_2 \lesssim 1 M_\odot$) is accreted onto a neutron star or black hole primary. It is commonly accepted that LMXBs in the galactic disc and halo are the end product of binary evolution (see the review by Verbunt & van den Heuvel 1995). From early X-ray studies it is known that the rate of occurrence of persistently bright ($L_X > 10^{36} \text{ erg s}^{-1}$) LMXBs in globular clusters is ~ 100 times higher than in other regions of our Galaxy (Katz 1975; Clark 1975). Therefore a different mechanism which enhances LMXB formation must operate in globular clusters. According to binary evolutionary models, it is currently believed that the high stellar densities and enhanced rates of star interaction in globular clusters provide a favourable environment for the formation of LMXBs via tidal capture through close encounters between neutron stars and ordinary stars (Fabian, Pringle & Rees 1975). So far, 13 persistently bright LMXBs have been discovered in globular clusters. Twelve of them, with a collection of their properties, are listed in tables 1 of Grindlay (1993) and Deutsch et al. (2000). The 13th object is the recently discovered M15 X-2 (White & Angelini 2001). Most of the globular cluster LMXBs are type-I X-ray burst

sources, indicating that the compact object is an accreting neutron star. The increased effort to identify their optical counterparts is a critical part in the process of obtaining the dynamical properties of these sources (see e.g. Deutsch et al. 2000). Furthermore, their study provides important information about the evolution of the host globular cluster since close binaries can have a dramatic effect on the cluster dynamics (Elson et al. 1987; Hut et al. 1992).

X2127+119 was one of the first X-ray sources identified in a globular cluster (Giacconi et al. 1974) and the first ever globular cluster LMXB optically identified (Aurière, Le Fèvre & Terzan 1984; Aurière et al. 1986, Charles, Jones & Naylor 1986). Located within 2 arcsec of the crowded core of M15 (NGC 7078), the optical counterpart, AC211, is a $V \sim 15$ magnitude variable star. This makes AC211 one of the optically brightest LMXBs. Soon after its discovery, a periodicity of 8.5 hr was observed in the optical (Ilovaisky et al. 1987, Naylor et al. 1987) and X-rays (Hertz 1987), and initially associated with the orbital period of the system. However, Ilovaisky et al. (1993) showed through further optical photometry that the true orbital period of AC211 is 17.1 hr. The best ephemeris to date is provided by Homer & Charles (1998). The optical light curve of AC211 exhibits the largest amplitude orbital modulation of any X-ray bi-

nary (1.8 mag in U), showing a symmetrical partial primary eclipse and a broad dipping structure centred at phase 0.5 (Ilovaisky et al. 1993; Homer & Charles 1998). AC211 has been also studied in the UV (see e.g. Naylor et al. 1988, 1992) and EUV (Callanan, Drake & Fruscione 1999).

The low X-ray to optical luminosity ratio ($L_X/L_{opt} \sim 20$) suggests that AC211 is an Accretion Disc Corona (ADC) source (see White & Holt 1982 for an outline of this model). The eclipse and dipping components of the light curves together with the orbital modulation of the X-ray absorption column density (Hert & Grindlay 1983, Ioannou et al. 2002a) can be easily explained if the inclination of AC211 is high. Then the secondary star and the outer asymmetric rim of the disc will partially obscure the ADC X-ray source causing the eclipse and dips, respectively. However, the detection by *Ginga* of an X-ray burst (with radius expansion) associated with AC211 implied that the compact object was a directly visible neutron star (Dotani et al. 1990; van Paradijs et al. 1990), a result apparently inconsistent with the ADC model. Recently, White & Angelini (2001), through observations with the *Chandra* X-ray Observatory have resolved X2127+119 into two X-ray sources: the LMXB associated with AC211 and a new persistent LMXB, M15 X-2. Both of these are separated by 2.7 arcsec. Since M15 X-2 is 1.6 times brighter in X-rays than AC211, its X-ray flux significantly contributes to the flux of the unresolved sources. This artificially increases the X-ray luminosity of AC211, contaminates the X-ray spectrum and reduces the amplitude of the orbital modulation in the X-ray light curve obtained in previous observations. Furthermore, since M15 X-2 shows no clear modulation in its X-ray light curve, it is reasonable to assume that it is a low-inclination LMXB and we can see the compact object directly. Thus the bright X-ray bursts observed by *Ginga* (Dotani et al. 1990) and *RXTE* (Smale 2001) can be associated with a neutron star in M15 X-2. These arguments provide a natural explanation for some of the AC211's unusual multi-wavelength properties and further strengthen the ADC scenario.

However, despite these extensive studies, many of the fundamental physical parameters of AC211 remain unknown. This is largely due to the fact that in AC211, as in most of the persistently bright LMXBs, the optical flux generated in the disc by X-ray reprocessing overwhelms the absorption line spectrum of the secondary star. This makes it difficult to measure the radial velocity curve of the secondary. The background contamination from the surrounding field stars in M15 represents an annoying extra problem. Optical spectroscopy of AC211 by Naylor et al. (1988) showed the presence of emission at HeII $\lambda 4686$, Balmer lines (overpowered by the background) and HeI absorption features. From an analysis of the HeI absorption features and assuming an origin in the outer accretion disc, they claimed a systemic velocity for AC211 blue-shifted by -150 ± 10 km s^{-1} with respect to the globular cluster. Such a high γ velocity suggested tidal interaction as the mechanism of formation of the binary system accompanied by subsequent cluster ejection. However, observations by Ilovaisky et al. (1989) clearly displayed variations in the velocity of the HeI feature which showed that it was not representative of the true AC211 systemic velocity. Two alternative explanations for the HeI $\lambda 4471$ velocity have been suggested: Fabian, Guilbert & Callanan (1987) pointed to outflowing mass above

the accretion disc as cause of the HeI absorption. In favour of this hypothesis was the discovery from *HST* observations of P-Cygni profiles in the H β and CIV $\lambda 1550$ emission lines (Downes, Anderson & Margon 1996; Ioannou et al. 2002b). On the other hand, Bailyn, Garcia & Grindlay (1989) argued that the blueshifted HeI can originate in an outflowing gas from the L_2 Lagrangian point owing to a common envelope in the binary system. However, recent re-analysis of previously published optical spectroscopy by van Zyl et al. (2002) shows an orbital modulation for the HeI $\lambda 4471$ inconsistent with this model (see also Callanan, Naylor & Charles 1990).

Furthermore, no definitive picture of the accretion disc structure for AC211 has emerged. So far, for example, the origin of the dipping behaviour observed at phase ~ 0.5 is unknown: it may be due to a bulge caused by the re-impact of a gas stream which overflows the initial impact with the accretion disc. The lack of reliable dynamical properties for this system and observational details of the disc structure motivated us to carry out phase-resolved spectroscopy of the HeII $\lambda 4686$ feature and the HeI absorption lines. We proceed by giving in Section 2 a detailed discussion of the observations and data reduction. In Section 3 the analysis of the spectra is presented. A discussion of our results and a possible model that could account for some of the properties of AC211 is given in Section 4. Finally, a summary of our conclusions is presented in Section 5.

2 OBSERVATIONS AND DATA REDUCTION

AC211 was observed with the 4.5-m Multiple Mirror Telescope (MMT) on Mount Hopkins in two runs during 1996 August 10-14 UT and August 31, September 1-2 UT. Despite the variable observing conditions and mediocre seeing throughout all the observing nights (with a seeing FWHM of about 2 arcsec), the nights were good enough for spectroscopic observations. For both runs, we used the Blue Channel Spectrograph equipped with the Loral 3072x1024 CCD and the 832 grooves mm^{-1} grating in second order. A $CuSO_4$ filter was used to block the first order light. This setting provided a spectral coverage of 1000 Å, a dispersion scale of 0.35 Å pix^{-1} and a spectral resolution of 1 Å FWHM. The slit was rotated at position angles which reduced contamination from nearby cluster stars and the spatial binning of the chip was carried out as a function of the seeing conditions. The exposure times were typically 600 and 900 seconds. HeNeAr arc lamp spectra were taken regularly through the nights in order to determine the wavelength calibration. A record of the observations and instrumental setup is provided in Table 1.

The images were bias and flat-field corrected with standard IRAF* routines. Spectra were extracted with the IRAF KPNOSLIT package. The extraction of AC211 spectra and four nearby field stars was a process necessarily interactive and it was repeated several times image by image until an optimum result was obtained. The apertures were edited for each star and sized to maximize the number of pixels contributing to the object. Next, the spectra profiles were

* IRAF is distributed by the National Optical Astronomy Observatories.

traced and the spectra were extracted without background subtraction because the slit did not include any sky region. Note that we expect a negligible sky contribution since the spectral interval observed is free of strong line bands (see e.g. Massey & Foltz 2000) and the main source of background is the unresolved globular cluster light and that from AC207 (Aurière & Cordoni 1981): the AC211 spectra presented here suffer considerably from contamination by the latter.

The pixel-to-wavelength calibration was derived from cubic spline fits to about 19 arc lines, giving a root-mean square deviation of typically $\lesssim 0.03 \text{ \AA}$. The wavelength scales of neighbouring arc spectra were interpolated in time and the accuracy of the whole process was checked by cross-correlation of the normalized sum of two field star spectra in the range $\lambda\lambda 4900 - 5000$ with the individual spectra of the corresponding star. The systematic velocity errors obtained from the scatter of the measured zero velocities were less than 3 and 5 km s^{-1} for the first and second run, respectively. Two spectra were rejected because they gave residual velocities of 7 and 4σ .

We also found that in a few cases the trace was lost when extracting the spectra. In general, this happened near the ends of the slit where the throughput of the spectrograph drops. We removed these regions in the spectra by masking them. On the night of September 1, we suffered difficulties because of condensation inside the CCD control box which introduced spurious negative features in the object and arc frame spectra. Because of that, we rejected this night from the analysis. Our final data set consists of 40 and 19 spectra of AC211 for the first and second run respectively.

For the subsequent spectra analyses we used the MOLLY package. The spectra were rebinned into a constant velocity scale and normalized by dividing them by the result of fitting a low order spline to the continuum after masking the Balmer absorption lines and the HeII $\lambda 4686$ emission line in the case of AC211. To fold the spectra on the orbital period, we used the linear ephemerides from Homer et al. (1998; 2002) to determine the orbital phases:

$$\phi = 0.0, JD = 2447790.964(2) \pm n \times 0.7130207(5) d$$

where $\phi = 0.0$ corresponds to closest approach of the secondary to the observer.

3 RESULTS

3.1 The mean spectrum

A comparison between the mean spectrum of AC211 over the two runs is shown in Fig. 1. The only feature in the spectrum with unquestionable origin from AC211 is the HeII $\lambda 4686$ emission line. For the first run, this line shows a full width zero intensity (FWZI) of 865 km s^{-1} , a FWHM= 516 km s^{-1} and a mean equivalent width (EW) of $1.0 \pm 0.3 \text{ \AA}$, with the error accounting (from now on) for line variability. The mean line shows a double-peaked profile with a peak-to-peak separation of $288 \pm 6 \text{ km s}^{-1}$ and enhanced emission on the blue-shifted peak. For the second run, we measured a FWZI= 800 km s^{-1} , a FWHM= 373 km s^{-1} and an EW= $0.6 \pm 0.1 \text{ \AA}$ for a line which shows no double peak profile. Note that the EW estimates in particular are underestimated because of contamination from AC207.

The spectral range observed was chosen to cover the

HeI absorption lines reported at $\lambda\lambda 4388, 4471, 4713, 4921$ by Naylor et al. (1988, 1989) and Ilovaisky (1989). A meticulous search for them in the mean and individual spectra was unsuccessful. An absorption feature at $\lambda 4469$ (rest frame wavelength) was discerned in the AC211 spectrum, but it is also present in the field stars (see Fig. 2), indicating that the absorption in AC211 is due to contamination from the globular cluster background. We suggest that this feature is (partial or totally) due to TiII $\lambda 4468.5$. Titanium lines are detected in the red giant members of M15 (see e.g. Cohen 1979; Sneden et al. 2000) and its abundance is even enhanced for Blue Horizontal Branch stars (Behr, Cohen & McCarthy 2000). We measure an equivalent width of $0.18 \pm 0.05 \text{ \AA}$ for the AC211 spectra and $0.19 \pm 0.03, 0.27 \pm 0.06, 0.24 \pm 0.03$ and $0.12 \pm 0.02 \text{ \AA}$ for the field stars (see Aurière & Cordoni 1981) AC160, AC11, AC623 and AC256 respectively.

Most of the absorption profile for the prominent H β line is also due to the background contamination, but we will show below that part of this line has its origin in the binary system.

3.2 Phase dependent and long-term profile variations

In order to examine the variability of the line profiles with orbital phase, we folded the HeII $\lambda 4686$ and the H β profiles into 15 orbital phase bins by using the ephemeris of Sec 2. Fig. 3 displays the results obtained for each run in the form of trailed spectrograms where two obvious features appear. In the upper-left panel, an S-wave is present in the HeII $\lambda 4686$ profiles. This line component reaches maximum blueshift around phase 0.75 and maximum redshift around 0.25, with intensity increasing relative to the continuum flux between orbital phases 0.68–0.94. The modulation in intensity explains the asymmetry in intensity of the red and blue components of the double-peaked emission for the first run when averaged over the orbit. Another interesting characteristic in the behaviour of the HeII $\lambda 4686$ profile is the absence of clear signs of rotational disturbance during the eclipse of the accretion disc by the donor star (which ranges in orbital phases from 0.8–0.15; Ilovaisky et al. 1993). The lack of a disturbance in the line implies that at least some of the emission is formed mainly in non-eclipsed vertical regions on or over the accretion disc.

The radial velocity curve and EWs of the HeII $\lambda 4686$ are plotted in Fig. 4. The radial velocities were determined by cross-correlation of each individual profile with a Gaussian template having the same width as the mean line for the corresponding run. In the case of the first run, these velocities are modulated clearly with phase, ranging from a minimum of -197 km s^{-1} to a maximum of -6 km s^{-1} . It is the S-wave, which moves and varies in strength across the profile, that is the cause of these variations, while the main body of the line shows no clear modulation.

The plot of the EW versus orbital phase shows that the EW is larger during the eclipse of the accretion disc by the secondary star, with higher EWs centered around phase 0.9 and lower EWs observed at phase ~ 0.3 . This behaviour suggests again that a considerable fraction of the HeII emitting region is not closely confined to the orbital plane: an intrinsically variable HeII line flux combined with an eclipse by the secondary of the continuum from the accretion disc

could explain the observed modulation in the EW. Nevertheless, the possibility of apparent EW variability introduced by seeing variations may also affect these measurements.

Despite the fact that a large fraction of the $H\beta$ line is due to the cluster background, the folded spectra in the upper-right panel of Fig. 3 show evidence for orbital motion and, therefore, for a contribution from AC211. In particular, this line develops a blue absorption wing around orbital phase 0.25. This is in contrast with the results of van Zyl et al. (2002) who found no clear dependence of the $H\beta$ line on the orbital cycle.

Because of poor orbital phase coverage, the observations during the second run (lower panels of Fig. 3) are of less use in trying to measure orbital or longer term variations in the line profiles. In this regard, the trailed spectra do not sample the S-wave component at HeII $\lambda 4686$ or the blue absorption wing at $H\beta$ adequately. Fortunately some information can still be extracted since the observations during both runs match at four phase intervals (0.0–0.07, 0.13–0.2, 0.4–0.47 and 0.53–0.67). Comparison of the HeII line profiles at the same phase intervals showed no recurrence of the profile shape. This result points to changes in the gas dynamics of the binary system over a time-scale of order a few days. Since the Rossi X-ray Timing Explorer All-Sky Monitor light curve of X2127+119 shows no significant variation in the X-ray flux/hardness ratio between both epochs of observation, we think it improbable that the differences observed above between the line profiles are due to changes in the degree of X-ray irradiation.

3.3 Doppler tomography

In order to gain insight into the HeII $\lambda 4686$ emitting regions in AC211, a tomogram of this line was constructed by using the Doppler tomography technique (Marsh and Horne 1988). We applied the maximum-entropy method of building the tomograms from the profiles obtained during the first run. Note that this technique was not used with the profiles from the second run due to the poorer orbital coverage (< 50%). Also we did not attempt to combine the data (in order to improve the orbital coverage) since there is evidence of long-term variations in the line profiles (Sec 3.2).

To obtain a reliable brightness distribution, the phase-resolved spectra acquired during the eclipse of the accretion disc by the secondary star should not be included (see e.g. Marsh & Horne 1990). However, because the eclipse appears to have no effect on the velocity profiles of the HeII $\lambda 4686$ line, we decided to build the map using the whole data set of 40 spectra. During the process of Doppler tomography, the γ velocity was adjusted to the cluster mean velocity (-107.8 km s $^{-1}$, Gebhardt et al. 1997). This value is in agreement with the velocities obtained by fitting a Gaussian to the average profile. We note that such a velocity for the HeII line, in agreement with the cluster velocity, argues against a high systemic velocity for AC211. Fig. 5 displays the resultant tomogram. The map shows a faint ring of emission (a signature of emission arising from a rotating accretion disc) and a region of enhanced intensity located at approximately $V_X = 30$ km s $^{-1}$, $V_Y = 160$ km s $^{-1}$. This tomogram should be considered an approximate reconstruction of the velocity dependent line brightness distribution, since it does not strictly satisfy the assumptions that underlie the Doppler

tomography technique, for example, that all motion is confined to the orbital plane or that all points in the system are equally visible at all times. In this regard, the image could also be affected by the inclusion of data observed during orbital phases 0.35–0.65, when the accretion disc may partially mask the secondary star (Ilovaisky et al. 1993).

4 DISCUSSION

Our HeII $\lambda 4686$ EWs are lower than the 1.7 Å reported by Baily, Garcia & Grindlay (1989) and considerably lower than the 9.7 Å measured by Downes et al. (1996) using *HST* observations. Since our observations were taken with inferior seeing than those referred to above, our spectra may be affected by higher background contamination which artificially increases the continuum. We attempted to decontaminate the MMT spectra of AC211 (out of eclipse) by subtracting different amounts of local background in an attempt to match the resulting continuum to the flux distribution of a black body of $T_{eff}=15,000$ K, found by Downes et al. (1996). This resulted in HeII $\lambda 4686$ EWs increasing only by a factor of two, still at least a factor of 5 lower than the values measured from the *HST* observations (note that the MMT spectrum we selected for comparison and the *HST* spectrum were both obtained at similar orbital phases). This result suggests that the differences observed in the measured EWs are intrinsic to AC211 and reflect long-term dramatic changes in the emitting regions. This may be related to the changes observed between the two runs in the overall averaged line profile and points to significant changes in the form of the gas flow in the system. Also, in comparison to previous observations, no HeI absorption lines are detected in the spectra (even after our attempts at decontamination), suggesting again long-term variability in the gas regions where these lines are formed. However, because of the lack of simultaneous X-ray observations, we cannot rule out the possibility that the differences in strength of the HeII $\lambda 4686$ line and the presence/absence of the HeI absorption lines may be caused partially or totally by changes in the flux or hardness of the X-ray flux (in contrast to the discussion in Sec 3.2).

Keeping in mind the caveats mentioned in the previous section concerning the Doppler image, we now discuss the possible origins of the HeII $\lambda 4686$. In contrast to the tomograms presented by van Zyl et al. (2002), it is clear that flux from the accretion disc contributes to this line. The tomogram (Fig. 5) shows a diffuse ring with low velocities (~ 200 km s $^{-1}$). This is consistent with emission from the outer parts of a high inclination accretion disc as expected from the observed eclipses in the optical light curve. A more striking question is the origin of the enhanced emission observed at $V_X = 30$ km s $^{-1}$, $V_Y = 160$ km s $^{-1}$. This bright region produces the S-wave component in the trailed spectra of the HeII line (Fig. 4), which reaches maximum velocity near phase 0.75 and minimum near phase 0.25. In this regard, our S-wave corresponds to the so-called component B observed by van Zyl et al. (2002) in their HeII $\lambda 4686$ trailed spectra. Since the orbital modulation of the radial velocities is that expected for emission arising from the X-ray heated face of the secondary star, we decided to overplot on the Doppler image different outlines of the Roche lobe of the secondary star in order to constrain the physical param-

ters of the system. Knowing the orbital period, the position and the outline of the Roche lobe were calculated firstly by varying the inclination angle of the system between 60 and 90 degrees and assuming that the primary star is a neutron star of mass $M_1 = 1.4 M_\odot$. By doing this, we were able to match (at least partially) the Roche lobe to the emission feature in the tomogram for the cases with mass ratios ranging $0.1 < q < 0.4$ and therefore for semiamplitudes of the secondary ranging between $190 < K_2 < 230 \text{ km s}^{-1}$. Fig. 5 displays the predicted positions of the Roche Lobe of the secondary star and the theoretical paths of the gas stream for an averaged mass ratio of $q = M_2/M_1 = 0.3$ and a semi-amplitude of the secondary of $K_2=210 \text{ km s}^{-1}$. Note that the masses implied for the secondary star of $0.1 < M_2 < 0.6 M_\odot$ are consistent with the range of masses obtained by applying the properties of a stripped giant to the secondary of AC211 (see Homer et al. 1998). Additionally, for a fixed inclination of 90 degrees we found that for $M_1 \geq 3 M_\odot$ the Roche lobe did not match the emission in the tomogram, which would suggest that the primary is a neutron star. However, these conclusions are based on the assumption that the S-wave arises from the secondary star: the fact that the S-wave component can sometimes be strong during the eclipse ingress (see upper panel Fig. 3), at the time when the X-ray irradiated face of the secondary (the expected main contributor to the S-wave component flux) points away from the observer, implies that the S-wave may not always originate on the secondary star and that the dynamical constraints obtained above should be treated with caution.

In addition, another result from the Doppler map is the absence of hotspot (the stream/disc impact region) expected at $V_X < 0, V_Y > 0$ and the lack of signs of reimpact of the gas stream in the lower quadrants ($V_Y < 0$). The latter is an unexpected result for AC211: as stated previously, one might hope that the broad dip centred at phase 0.5 in the optical light curve could be due to occultation of the ADC/accretion disc by a bulge at the rim of the accretion disc caused by the reimpact of outflowing gas (see Sec 1). This map does not appear to support this interpretation unless the hotspot and the region of reimpact are fainter or comparable in brightness to the accretion disc at HeII $\lambda 4686$.

Nonetheless, it is tempting to associate the unusual spectroscopic properties of AC211 with its origin via tidal capture. Immediately after formation it is likely that the secondary was misaligned with respect to the orbital angular momentum vector. If the secondary spin and the orbital angular momentum vectors are not yet aligned, the gas stream will leave the inner Lagrangian point of the donor star with an additional kinematical contribution in the direction perpendicular to the orbital plane (see e.g. Lanzafame, Belvedere & Molteni 1994) and travel a distance above the orbital plane considerably larger than the vertical height of the accretion disc. Hence, the gas stream will be visible (generating the enhanced emission in the Doppler map), travel without interaction with the outer edge of the accretion disc, and fall back to the disc, hitting its inner side. Thus the impact of the gas stream will create a bulge which may cause the dip in the light curves centred at phase 0.5 with no observable bright spot since the hot regions are not dominant at HeII $\lambda 4686$ and/or they are obscured by the outer disc. In this scenario, the variations observed in the intensity of the S-wave and the long-term changes in the

HeII line profiles are due to long term changes in the accretion geometry attributable in turn to a precessing secondary star. Indeed, there is some observational evidence for binary stars with one component rotating asynchronously and with a misaligned spin (Głęboczi & Stawikowski 1997).

Although this is an interesting model, the current theories of tidal evolution of close binary systems predict that the alignment between the orbital axis and the rotational axis of a secondary with a convective envelope should occur earlier than or at a similar time to the circularization of the orbit (see Hut 1981, Eggleton & Kiseleva-Eggleton 2001). In particular, the tidal circularization time-scale for AC211 is estimated to be a few hundred years (Eggleton 2002). Therefore it is highly improbable that we are observing a misaligned secondary star unless the system has been formed recently or the secondary underfills its Roche lobe (both unlikely scenarios).

5 SUMMARY AND CONCLUSIONS

In this paper we have presented time-resolved optical spectroscopy of AC211/X2127+119. Our Doppler tomogram of the HeII $\lambda 4686$ line shows enhanced emission at $V_X = 30 \text{ km s}^{-1}$, $V_Y = 160 \text{ km s}^{-1}$ superimposed on emission arising from the accretion disc. The phasing (if not the intensity modulation) of this emission suggests an origin on the irradiated face of the secondary. This in turn implies that AC211 is a high mass ratio system ($0.1 < q < 0.4$). Furthermore, the Doppler map suggests a neutron star primary and a low mass secondary star of mass $0.1 < M_2 < 0.6 M_\odot$. We observe that the HeII $\lambda 4686$ shows considerable variation in its line profile on a time-scale of order a few days clearly unrelated to any orbital modulation. These have also been noted by van Zyl et al. (2002). Further observations are required in order to understand these changes in the emitting gas structure. Although a misaligned secondary (as might be expected immediately after tidal capture) may provide a natural explanation of some of the phenomena observed here, it is excluded on the basis of the short circularization time-scale of the orbit.

6 ACKNOWLEDGEMENTS

Use of *MOLLY*, *DOPPLER* and *TRAILER* developed largely by T. R. Marsh is acknowledged. We are grateful to P. Garnavich and R. P. Kirshner for generously obtaining some of the data used in this paper. We thank Craig Foltz for helpful comments during the data reduction, Lee Homer for providing the AC211 linear ephemeris, A. Recio-Blanco for confirming the presence of TiII $\lambda 4468.5$ in Horizontal-Branch stars in M15 and P. Eggleton for his remarks about the possible tidal evolution of AC211. We also thank the anonymous referee for useful comments.

REFERENCES

- Aurière M., Cordoni J.-P., 1981, A&AS, 46, 347
- Aurière M., le Fèvre O., Terzan A., 1984, A&A, 138, 415
- Aurière M., Maucherat A., Cordoni J.-P., Fort B, Picat J. P., 1986, A&A, 158, 158

- Bailyn C. D., Garcia M., Grindlay J. E., 1989, *ApJ*, 344, 786
- Behr B. B., Cohen J. G., McCarthy J. K., 2000, *ApJ*, 531, 37
- Callanan P. J., Naylor T., Charles P. A., 1990, in Mauche C. W., eds, *Accretion-Powered Compact Binaries*. Cambridge University Press, Cambridge, p. 51
- Callanan P. J., Drake J. J., Fruscione A., 1999, *ApJ*, 521, L125
- Charles P. A., Jones D. C., Naylor T., 1986, *Nat.*, 323, 417
- Clark G. W., 1975, *ApJ*, 199, L143
- Cohen J. G., 1979, *ApJ*, 231, 751
- Deutsch E. W., Margon B., Anderson F. S., 2000, *ApJ*, 530, L21
- Dotani T., Inoue H., Murakami T., Nagase F., Tanaka Y., 1990, *Nat.*, 347, 534
- Downes R. A., Anderson S. F., Margon B., 1996, *PASP*, 108, 688
- Eggleton P. P., Kiseleva-Eggleton L., 2001, *ApJ*, 562, 1012
- Eggleton P., 2002, private communication
- Elson R., Hut P., Inagaki S., 1987, *ARAA*, 25, 565
- Fabian A. C., Pringle J. E., Rees M. J., 1975, *MNRAS*, 172, 15P
- Fabian A. C., Guilbert P. W., Callanan P. J., 1987, *MNRAS*, 225, 29P
- Glębocki R., Stawikowski A., 1997, *A&A*, 328, 579
- Gebhardt K., Pryor C., Williams T. B., Hesser J. E., Stetson P. B., 1997, *ApJ*, 113, 1026
- Giacconi R., Murray S., Gursky H., Kellogg E., Schreier E., Matilsky T., Koch D., Tananbaum H., 1974, *ApJS*, 27, 37
- Grindlay J. E., 1993, *The Globular Cluster-Galaxy Connection*, ed. Graeme H. S. and Brodie J. P., *ASP*, 48, 156
- Hertz P., Grindlay J. E., 1983, *ApJ*, 275, 105
- Hertz P., 1987, *ApJ*, 315, L119
- Homer L., 2002, private communication
- Homer L., Charles P. A., 1998, *New Astron.*, 3, 435
- Hut P., 1981, *A&A*, 99, 126
- Hut P., McMillan S. L. W., Goodman J., Mateo M., Phinney E. S., Pryor C., Richer H. B., Verbunt F., Weinberg M., 1992, *PASP*, 104, 981
- Ilovaisky S. A., Aurière M., Kock-Miramond L., Chevalier C., Cordoni J. P., 1987, *A&A*, 179, L1
- Ilovaisky S. A., 1989, *Proc of the 23rd ESLAB Symposium on Two Topics in X-ray Astronomy*, Volume 1, p. 145
- Ilovaisky S. A., Aurière M., Koch-Miramond L., Chevalier C., Cordoni J. P., Crowe R. A., 1993, *A&A*, 270, 139
- Ioannou Z., Naylor T., Smale A. P., Charles P. A., Mukai K., 2002a, *A&A*, 382, 130
- Ioannou Z., Naylor T., van Zyl L., Charles P. A., Smale A. P., Mukai K., 2002b, in Gänsicke B. T., Beuermann K. & Reinsch K., eds, *ASP Conf. Ser. Vol. 261, The Physics of Cataclysmic Variables and Related Objects*. Astron. Soc. Pac., San Francisco, p. 351
- Katz J. I., 1975, *Nat.*, 253, 698
- Lanzafame G., Belvedere G., Molteni D., 1994, *MNRAS*, 267, 312
- Marsh, T. R., Horne K., 1988, *MNRAS*, 235, 269
- Marsh, T. R., Horne K., 1990, *ApJ*, 349, 593
- Massey P., Foltz C., 2000, *PASP*, 112, 566
- Naylor T., Charles P. A., Drew J. E., Hassall B. J. M., 1988, *MNRAS*, 233, 285
- Naylor T., Charles P. A., 1989, *MNRAS*, 236, 285
- Naylor T., Charles P. A., Hasall B. J. M., Raymond J. C., Nasiopoulos G., 1992, *MNRAS*, 255, 1
- Smale A. P., 2001, *ApJ*, 562, 957
- Snedden C., Johnson J., Kraft R. P., Smith G. H., Cowan J. J., Bolte M. S., 2000, *ApJ*, 536, 85
- van Paradijs J., Dotani T., Tanaka Y., Tsuru T., 1990, *PASJ*, 42, 633
- van Zyl L., Naylor T., Charles P. A., Ioannou Z., to appear in *MNRAS*
- Verbunt F., Van den Heuvel E. P. J., 1995, in Lewin W. H. G., van Paradijs J. & van den Heuvel E. P. J., eds, *X-Ray Binaries*. Cambridge University Press, Cambridge, p. 457
- White N. E., Holt S. S., 1982, *ApJ*, 257, 318
- White N. E., Angelini L., 2001, *ApJ*, 561, L101

Table 1. Journal of Observations.

Date (UT)	No. spectra	HJD start (+2,450,000.)	HJD end (+2,450,000.)	λ range (\AA)	Spatial Scale ^a (arcsec/pix)	Slit Width (arcsec)
10/08/96	9	305.7836	305.9164	4240-5190	0.3	1
11/08/96	6	306.8062	306.9930	"	"	"
12/08/96	21	307.7018	307.9941	4335-5282	"	"
13/08/96	5	308.7966	308.8337	4253-5190	0.6	"
14/08/96	9	309.7753	309.8507	"	0.6	"
31/08/96	17	326.7333	326.9509	4236-5179	"	1.25
01/09/96	4	327.6787	327.8672	4388-5330	"	"
02/09/96	6	328.6290	328.9550	"	"	"

^a: the nominal unbinned scale is 0.3 arcsec/pix.

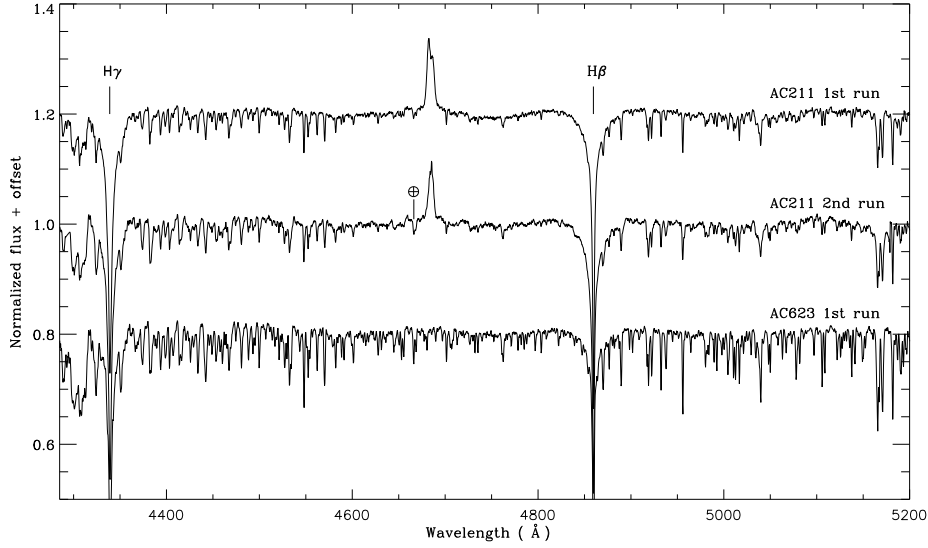


Figure 1. Normalized mean spectra of AC211 for the first (top) and second (middle) runs, together with the mean spectrum of the field star AC623 (bottom). The AC211 spectrum shows the clear presence of He II $\lambda 4686$ in emission and weak absorption features. The latter are totally due to background contamination from neighbouring stars. \oplus marks an instrumental feature poorly removed by the flat field correction for the second run.

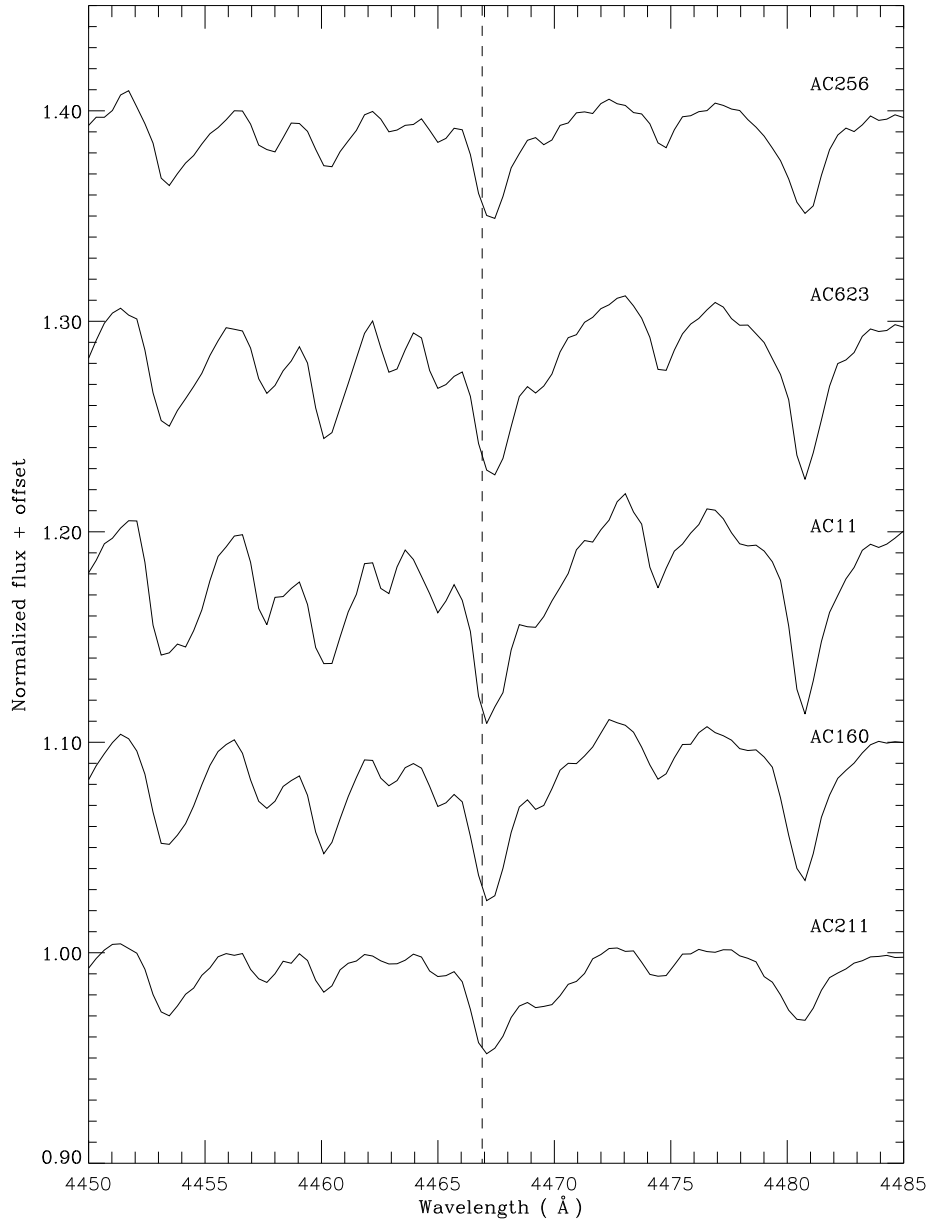


Figure 2. Enlargement at $\lambda 4471$ for the mean spectrum of AC211 and its neighbours. The dashed line marks the expected position of the TiII $\lambda 4468.5$ absorption line at the globular cluster rest frame.

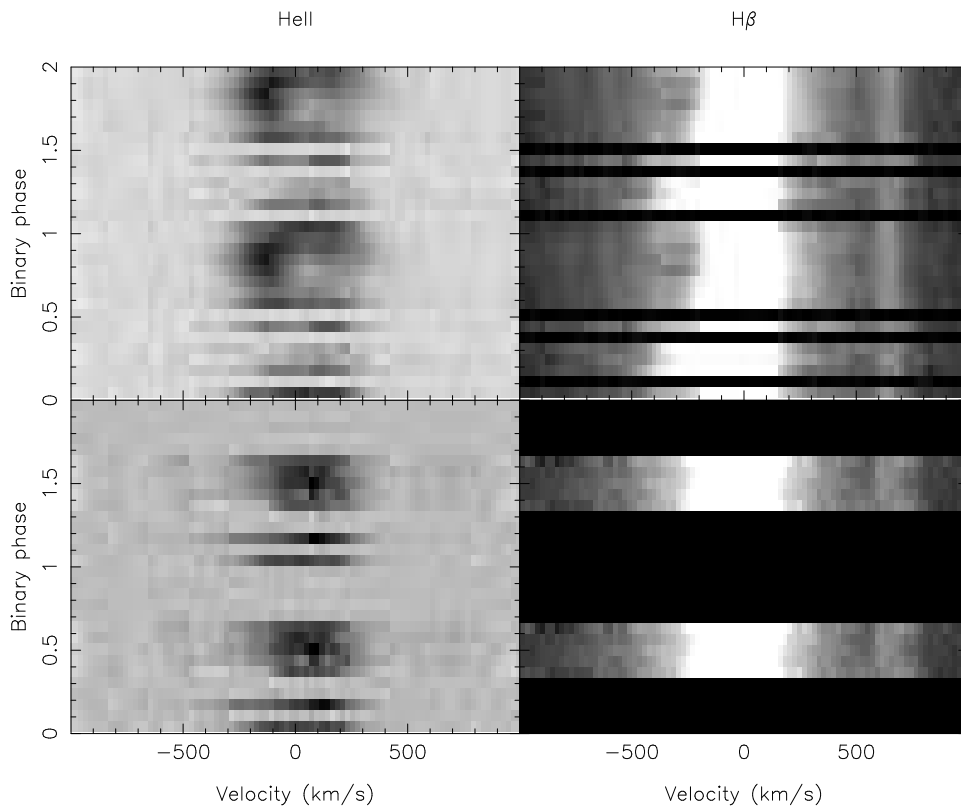


Figure 3. Trailed spectrograms of HeII $\lambda 4686$ and H β for the first (upper panels) and second (lower panels) run. For the sake of clarity, the same cycle has been plotted twice. Empty strips represent gaps in the phase coverage. Zero velocity corresponds to the laboratory wavelength. The grey scale shows emission lines in black and absorption lines in white. The scale in the H β trailed spectrogram was chosen in order to outline the blue wing absorption component of the line. Note that for the second run, we removed the data acquired during the night of September 2 because the H β profile fell on a bad column in the CCD chip.

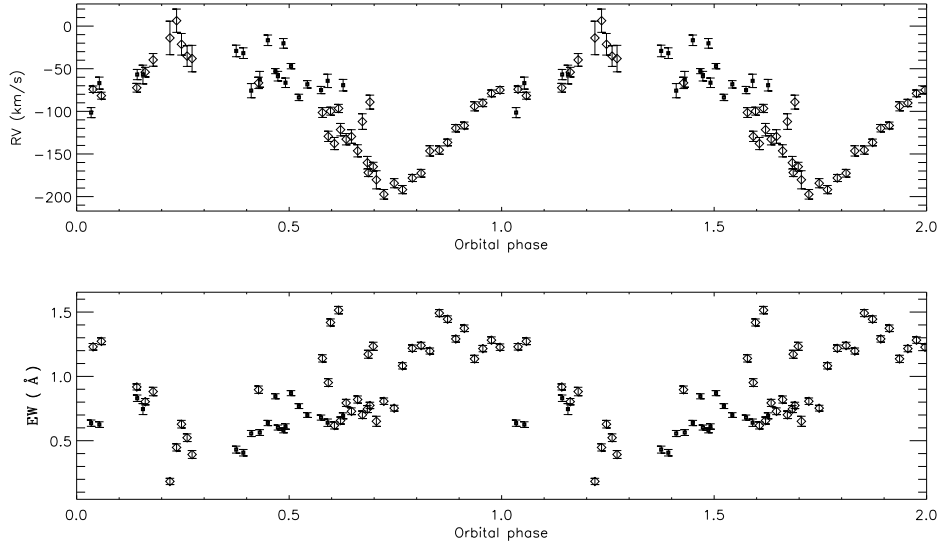


Figure 4. Radial velocities (upper panel) and EW (lower panel) of He II $\lambda 4686$ folded on the ephemeris of Sec. 2. Diamonds and solid squares correspond to the first and second run respectively. The same cycle has been plotted twice.

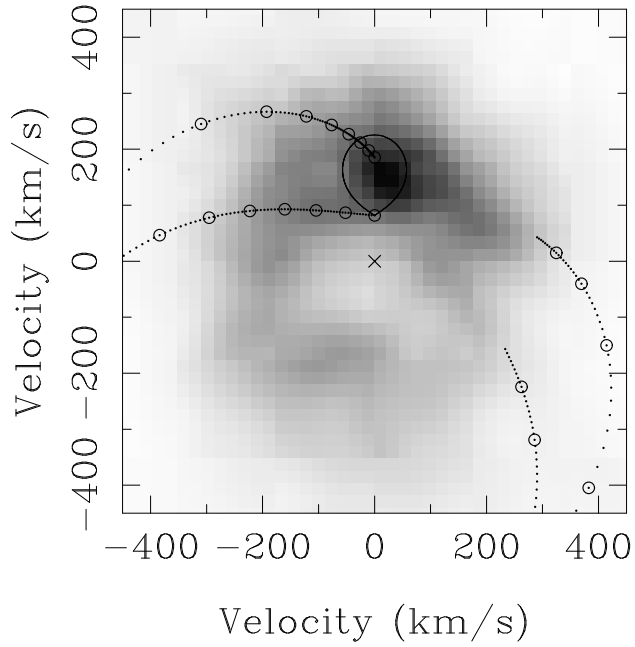


Figure 5. Doppler map of HeII $\lambda 4686$ computed by using the whole 40 spectra from the first run. The Roche lobe of the secondary star, the predicted velocities of the gas stream (lower curve) and of the disc along the gas stream (upper curve) are plotted for $K_2 = 210 \text{ km s}^{-1}$ and $q = M_2/M_1 = 0.3$. Distances in units of $0.1R_{L1}$ are marked along both curves with open circles. The centre of mass of the system is denoted by a cross.